Contribution from the Department of Chemistry and Laboratory for Molecular Structure and Bonding, Texas A&M University, College Station, Texas 77843

Unbridged M–M Multiple Bonds in the $Cr_2(tmtaa)_2$ and $Mo_2(tmtaa)_2$ Molecules (tmtaa = Dianion of 7,16-Dihydro-6,8,15,17-tetramethyldibenzo[*b*,*i*][1,4,8,11]tetraazacyclotetradecine): Experimental and Theoretical Investigations

F. Albert Cotton,* Joanna Czuchajowska, and Xuejun Feng

Received April 6, 1990

The title compounds have been prepared, their molecular structures determined by X-ray crystallography, and their electronic structures calculated by the SCF–Xα–SW method. The chromium compound (I) was obtained by two methods that are different from any previously reported while the molybdenum compound was made by the reaction of $Mo_2(O_2CCH_3)_4$ and Li_2tmtaa, previously mentioned but not described in detail. The two compounds are isomorphous ($P\bar{1}$, $Z = 2$) with the following unit cell dimensions (I followed by II in each case): a = 11.707 (4), 11.743 (6) Å; b = 16.436 (5), 16.716 (9) Å; c = 11.571 (3), 11.680 (8) Å; α = 90.39 (3), 90.87 (6)°; β = 107.13 (3), 106.81 (5)°; γ = 108.85 (3), 108.36 (5)°. The molecules are very similar, each having the two saddle-shaped ligands rotated 90° to each other. For I, the Cr atoms are ca. 0.50 Å above the N_4 planes with Cr–Cr = 2.101 (1) Å; for II, the corresponding numbers are 0.55 and 2.175 (1) Å. Both M–M distances are greater than those previously found for M_2^{4+} units in an M_2X_8 framework without axial interactions. The SCF–Xα–SW calculations show that little if any Cr–Cr δ bonding exists whereas there is a significant amount of δ bonding in the molybdenum compound. The relatively small (0.074 Å) difference between the Cr–Cr and Mo–Mo distances (0.11–0.22 Å being the previously known range) is discussed.

Introduction

Of the many problems posed by the chemistry of compounds with multiple bonds between metal atoms,[1] one of the most fascinating and intensively studied concerns the great difference between the compounds formally based on the quadruply bonded Cr_2^{4+} unit and those of Mo_2^{4+}. This problem has been of particular concern to workers in this laboratory, where nearly all of the compounds containing strong Cr–Cr bonds were discovered and characterized. As a natural extension of our long-standing program in this area, we undertook the work described in this paper several years ago, upon learning that the compound $Mo_2(tmtaa)_2$ could be prepared[2] (tmtaa is an abbreviation for the dianion $C_{22}H_{22}N_4^{2-}$, whose systematic name appears in the title and whose structure is shown in Figures 2 and 3).

Those who first reported $Mo_2(tmtaa)_2$ showed that it could be oxidized and reduced to give the stable cation and anion, respectively, and they also gave a brief account of the structure of the cation. The cation was found to have a structure with D_{2d} symmetry with each Mo atom displaced 0.57 Å from the nearest N_4 plane and an Mo–Mo distance of 2.221 (1) Å. Several questions were prompted by these observations:

(1) How will the Mo–Mo distance in the neutral molecule compare with that in the cation?

(2) Can the chromium analog, $Cr_2(tmtaa)_2$, be prepared, and if so, what will its structure be?

(3) With the aid of rigorous molecular orbital calculations, can we develop an understanding of the bonding in each of these molecules with particular emphasis on the comparison between them?

To our great delight, we quickly found that $Cr_2(tmtaa)_2$ does exist and can, in fact, be easily prepared in several ways. Ironically, since the isolation and structure determination of the chromium compound had been anticipated to be the most problematical and uncertain of the three phases of the projected research, it was the formation of good crystals of $Mo_2(tmtaa)_2$ and the convergence of the MO calculations that took the most time. However the entire study is now complete and is reported here. In the meantime, a preliminary report on the chromium compound has been published.[3]

Experimental Section

Materials and Methods. All manipulations were carried out under an argon atmosphere, using standard vacuum-line and Schlenk techniques. The solvents were freshly distilled under nitrogen from the appropriate drying agents. Butyllithium and chromocene were obtained from Aldrich. Starting materials, $Cr_2(O_2CCH_3)_4$,[4] $Mo_2(O_2CCH_3)_4$[5] and H_2tmtaa,[6] were prepared according to the literature.

Preparation of $Cr_2(tmtaa)_2$. Method A. $Cr_2(O_2CCH_3)_4$, 0.05 g (0.15 mmol), was suspended in 8 mL of THF at −10 °C. To this was added a solution of 0.3 mmol of the lithium tmtaa salt in 10 mL of THF at −10 °C via cannula (the salt was prepared by reacting 0.1 g of H_2tmtaa (0.3 mmol) with 0.37 mL of 1.6 M *n*-BuLi in 10 mL of THF). The reaction solution was stirred at room temperature for 4 h and then filtered through Celite. The filtrate was evaporated to dryness, and the remaining solid was dissolved in 16 mL of toluene. This deep red solution was filtered through Celite and carefully layered with 20 mL of hexanes. In 48 h, large blocklike crystals had formed on the bottom of the Schlenk tube. The crystals contain an interstitial hexane molecule (as shown by X-ray crystallography). ^{1}H NMR (C_6D_6): δ 1.99 (s, CH_3), 4.25 (s, γ-CH) and 6.90 (m, ArH). Some additional resonances were present in the region 0.8–1.5 ppm due to the free hexane molecule. (All peaks were broad.)

Method B. Cp_2Cr, 0.06 g (0.33 mmol), and H_2tmtaa, 0.11 g (0.33 mmol), were dissolved in 16 mL of toluene at room temperature. The reaction solution was stirred for 1 h, becoming deep orange/red in color. After that, the solution was refluxed vigorously for 24 h, cooled to room temperature, and filtered twice through Celite (to get rid of some jellylike light brown residue). The resulting deep orange solution was layered with 20 mL of isomeric hexanes. In 48 h, nice, blocklike crystals had formed on the bottom of the Schlenk tube. Unit cell dimensions were as follows (different from above): triclinic, space group $P\bar{1}$ with a = 11.61 Å, b = 14.84 Å, c = 15.55 Å, α = 96.93°, β = 102.13°, γ = 107.50°, V = 2450 Å^3. These dimensions agree with the ones reported elsewhere.[3]

Formation of Cr(tmtaa)Cl. Due to some $CrCl_3$ impurities, presumably contained in chromocene, one can also obtain via method B a few single crystals of Cr(tmtaa)Cl, a compound previously synthesized and characterized by us.[7] Unit cell dimensions are as follows: triclinic, space group $P\bar{1}$ with a = 8.697 (4) Å, b = 10.917 (5) Å, c = 12.900 (7), α = 77.14 (4)°, β = 77.24 (4)°, γ = 75.67 (4)°, and V = 1139 (1) Å^3. These dimensions are different from the ones previously published by us[7] due to the presence of one interstitial cyclopentadiene molecule. The Cr(tmtaa)Cl molecule is virtually identical in the two crystalline forms.

Preparation of $Mo_2(tmtaa)_2$. $Mo_2(O_2CCH_3)_4$, 0.05 g (0.12 mmol), was suspended in 10 mL of THF at −10 °C. To this was added a solution

(1) (a) Cotton, F. A.; Walton, R. A. *Multiple Bonds Between Metal Atoms*, John Wiley & Sons, 1982; Chapters 3 and 4. (b) Cotton, F. A.; Walton, R. A. *Structure and Bonding*, **1985**, *62*, 1.
(2) Mandon, D.; Giraudon, J.-M.; Toupet, L.; Sala-Pala, J.; Guerchais, J. E. *J. Am. Chem. Soc.* **1987**, *109*, 3490.
(3) Edema, J. J. H.; Gambarotta, S.; van der Sluis, P.; Smeets, W. J. J.; Spek, A. L. *Inorg. Chem.* **1989**, *28*, 3782.
(4) Ocone, L. R.; Block, B. P. *Inorganic Syntheses* McGraw-Hill: New York, 1966; Vol. 8, pp 125–130.
(5) Stephenson, T. A.; Bannister, E.; Wilkinson, G. *J. Chem. Soc.* **1964**, 2538.
(6) Goedken, V. L.; Molin-Case, J.; Whang, Y.-A. *Chem. Commun.* **1973**, 337.
(7) Cotton, F. A.; Czuchajowska, J.; Falvello, L. R.; Feng, X. *Inorg. Chim. Acta* **1990**, *172*, 135.

0020-1669/90/1329-4329$02.50/0

Table I. Crystal Data for $M_2(C_{22}H_{22}N_4)_2 \cdot {}^1/_2C_6H_{14}$ (M = Cr, Mo)

formula	$Cr_2N_8C_{47}H_{51}$	$Mo_2N_8C_{47}H_{51}$
fw	831.98	919.86
space group	$P\bar{1}$	$P\bar{1}$
a, Å	11.707 (4)	11.743 (6)
b, Å	16.436 (5)	16.716 (9)
c, Å	11.571 (3)	11.680 (8)
α, deg	90.39 (3)	90.87 (6)
β, deg	107.13 (2)	106.81 (5)
γ, deg	108.85 (3)	108.36 (5)
V, Å^3	2000 (1)	2069 (2)
Z	2	2
d_{calc}, g/cm^3	1.381	1.477
μ(Mo Kα), cm^{-1}	5.730	6.337
radiation monochromated in incident beam (λ(Mo Kα), Å)	0.710 73	0.710 73
temp, °C	23 ± 1	23 ± 1
transm factors: max; min	1.00; 0.91	1.00; 0.96
R^a	0.0499	0.0487
$R_w{}^b$	0.0693	0.0627

$^a R = \sum||F_o| - |F_c||/\sum|F_o|$. $^b R_w = [\sum w(|F_o| - |F_c|)^2/\sum w|F_o|^2]^{1/2}$; $w = 1/\sigma^2(|F_o|)$.

of 0.24 mmol of the lithium tmtaa salt in 6 mL of THF at −10 °C via cannula (the salt was prepared by reacting 0.08 g of H_2tmtaa (0.23 mmol) with 0.29 mL of 1.6 M *n*-BuLi in 6 mL of THF). The reaction solution was stirred at room temperature for 12 h and then filtered through Celite. The brown filtrate was evaporated to dryness, and the remaining solid was dissolved in 14 mL of toluene. This solution was filtered through Celite into a three-neck flask equipped with a condenser and gently refluxed for 24 h. After that, the solution was cooled to room temperature, filtered through Celite, and carefully layered with 20 mL of hexanes. In 24 h, well-formed, blocklike, black/brown crystals had formed on the walls of the Schlenk tube. The crystals contain an interstitial hexane molecule (as shown by ^{1}H NMR and X-ray crystallography). UV–vis (toluene solution, nm): 431 and 346.

Measurements. The instruments used were as follows: Cary 17D for UV–vis spectra; Varian XL-200 for ^{1}H NMR spectra. Normal operating procedures were employed.

X-ray Crystallography. Cr_2(tmtaa)$_2$. Single crystals of Cr_2(tmtaa)$_2$ were grown by layering a toluene solution of the compound with hexanes. These crystals are air-sensitive and decompose within an hour upon exposure to the atmosphere. A blocklike red crystal was selected from the product and was shown to be of good quality by polarized-light microscopy. The crystal was coated with epoxy and mounted on the goniometer head of a Rigaku AFC5R diffractometer. Indexing revealed a triclinic cell, and the axial dimensions were confirmed with oscillation photographs. The data were collected with a constant speed of 4°/min in ω. Each scan was repeated four times or until $F/\sigma(F)$ reached 30, whichever came first. The data were collected to 46° in 2θ. Data were corrected for Lorentz and polarization effects[8] and absorption.[9] The empirical absorption correction made was based on ψ scans of several reflections with Eulerian χ angle near 90°. The structure was solved by standard heavy-atom methods. The subsequent development of the structure was done by an alternating sequence of least-squares refinements and difference Fourier maps. All non-hydrogen atoms were treated anisotropically, with the exception of the solvent molecule. This hexane molecule resides on an inversion center with the two terminal carbon atoms disordered over two positions. The molecule was modeled successfully by assigning 0.5 occupancy to the two carbon atoms. All hydrogen atoms were located in difference maps and refined with an overall isotropic temperature factor. Restraints were put on nine C–H interatomic distances and added to the least-squares refinements. The final cycle of full-matrix refinement (which was done in two blocks of 360 and 380 parameters, respectively) gave $R = 0.0499$ and $R_w = 0.0693$. Crystallographic and procedural data are presented in Table I, and the atomic positional parameters are given in Table II.

Mo_2(tmtaa)$_2$. The crystals were found to be isomorphous with those of the chromium compound as obtained in preparative procedure A. All procedures for collection and reduction of data were as just described. The structure was solved by standard heavy-atom methods. The subsequent development of the structure was done by an alternating sequence of least-squares refinements and difference Fourier maps. All atoms, including the solvent molecule, were treated anisotropically. This hexane molecule resides on an inversion center (as in the case of the chromium dimer; however, no disorder of the two terminal carbon atoms was observed). The final cycle of full-matrix refinement gave $R = 0.0487$ and $R_w = 0.0627$. Crystallographic and procedural data are presented in Table I, and the atomic positional parameters are given in Table III.

Computational Procedures. The present electronic structure study for the Cr_2(tmtaa)$_2$ and Mo_2(tmtaa)$_2$ molecules is based on molecular orbital calculations by the SCF–Xα–SW method for a model system. In this model system, the bulky macrocyclic tmtaa ligand was simplified to that shown as **1**. The atomic coordinates of each model molecule were determined from the crystal structure of the corresponding real molecule, and the relevant bond distances, bond angles, and dihedral angles were averaged to conform to D_{2d} idealized symmetry. A coordinate system (Figure 1) was defined with the Z axis colinear with the M–M bond and

Table II. Positional and Equivalent Isotropic Thermal Parameters and Their Estimated Standard Deviations for Cr_2(tmtaa)$_2$

atom	x	y	z	B,^{a} Å^2
Cr(1)	0.88509 (5)	0.16081 (4)	0.40646 (5)	1.84 (2)
Cr(2)	0.94302 (6)	0.29461 (4)	0.39405 (5)	2.01 (2)
N(1)	0.8583 (3)	0.1050 (2)	0.2410 (3)	2.09 (9)
N(2)	0.6975 (3)	0.1248 (2)	0.3795 (3)	2.14 (9)
N(3)	0.8835 (3)	0.1524 (2)	0.5781 (3)	2.16 (9)
N(4)	1.0449 (3)	0.1316 (2)	0.4414 (3)	2.01 (9)
N(5)	0.7848 (3)	0.3263 (2)	0.3428 (3)	2.5 (1)
N(6)	0.9933 (3)	0.3516 (2)	0.5641 (3)	2.4 (1)
N(7)	1.1324 (3)	0.3295 (2)	0.4393 (3)	2.39 (9)
N(8)	0.9188 (3)	0.2986 (2)	0.2159 (3)	2.34 (9)
C(1)	0.7479 (4)	0.0541 (3)	0.1653 (3)	2.4 (1)
C(2)	0.6325 (4)	0.0377 (3)	0.1894 (4)	2.8 (1)
C(3)	0.6072 (4)	0.0679 (3)	0.2904 (4)	2.5 (1)
C(4)	0.6772 (4)	0.1587 (3)	0.4825 (4)	2.5 (1)
C(5)	0.5749 (4)	0.1854 (3)	0.4809 (5)	3.4 (1)
C(6)	0.5734 (5)	0.2250 (4)	0.5855 (5)	4.1 (2)
C(7)	0.6736 (5)	0.2409 (3)	0.6912 (5)	3.9 (2)
C(8)	0.7763 (5)	0.2167 (3)	0.6940 (4)	3.1 (1)
C(9)	0.7790 (4)	0.1745 (3)	0.5912 (4)	2.5 (1)
C(10)	0.9557 (4)	0.1203 (3)	0.6620 (3)	2.3 (1)
C(11)	1.0573 (4)	0.1004 (3)	0.6458 (4)	2.6 (1)
C(12)	1.1013 (4)	0.1048 (3)	0.5439 (3)	2.1 (1)
C(13)	1.0804 (4)	0.1337 (3)	0.3338 (3)	2.2 (1)
C(14)	1.2049 (4)	0.1571 (3)	0.3286 (4)	2.8 (1)
C(15)	1.2274 (5)	0.1624 (3)	0.2174 (4)	3.5 (1)
C(16)	1.1285 (5)	0.1483 (4)	0.1107 (4)	3.6 (2)
C(17)	1.0054 (4)	0.1280 (3)	0.1136 (4)	2.8 (1)
C(18)	0.9791 (4)	0.1195 (3)	0.2238 (3)	2.2 (1)
C(19)	0.7377 (5)	0.0027 (4)	0.0513 (5)	4.1 (2)
C(20)	0.4740 (4)	0.0252 (4)	0.2955 (5)	3.8 (2)
C(21)	0.9269 (6)	0.0968 (4)	0.7795 (4)	3.7 (2)
C(22)	1.2092 (4)	0.0709 (3)	0.5576 (5)	3.0 (1)
C(23)	0.7603 (4)	0.3824 (3)	0.4053 (4)	2.9 (1)
C(24)	0.8340 (4)	0.4178 (3)	0.5248 (4)	3.3 (1)
C(25)	0.9424 (4)	0.4045 (3)	0.6003 (4)	3.0 (1)
C(26)	1.1070 (4)	0.3401 (3)	0.6346 (4)	2.7 (1)
C(27)	1.1410 (5)	0.3295 (3)	0.7580 (4)	3.6 (1)
C(28)	1.2488 (5)	0.3101 (4)	0.8143 (5)	4.4 (2)
C(29)	1.3247 (5)	0.2987 (4)	0.7477 (5)	4.5 (2)
C(30)	1.2917 (4)	0.3077 (3)	0.6241 (5)	3.6 (1)
C(31)	1.1844 (4)	0.3283 (3)	0.5658 (4)	2.7 (1)
C(32)	1.1998 (4)	0.3583 (3)	0.3630 (4)	3.0 (1)
C(33)	1.1409 (4)	0.3566 (3)	0.2379 (4)	3.3 (1)
C(34)	1.0146 (4)	0.3309 (3)	0.1682 (4)	3.0 (1)
C(35)	0.7882 (4)	0.2744 (3)	0.1506 (4)	2.8 (1)
C(36)	0.7258 (5)	0.2304 (3)	0.0340 (4)	3.4 (1)
C(37)	0.5948 (5)	0.2054 (3)	−0.0153 (5)	4.0 (2)
C(38)	0.5236 (5)	0.2216 (4)	0.0515 (5)	4.2 (2)
C(39)	0.5821 (4)	0.2624 (3)	0.1692 (5)	3.8 (2)
C(40)	0.7138 (4)	0.2904 (3)	0.2209 (4)	2.9 (1)
C(41)	0.6566 (6)	0.4205 (5)	0.3481 (6)	5.1 (2)
C(42)	1.0047 (6)	0.4611 (4)	0.7214 (5)	4.3 (2)
C(43)	1.3426 (5)	0.3985 (4)	0.4072 (5)	4.3 (2)
C(44)	0.9883 (6)	0.3468 (4)	0.0356 (5)	4.4 (2)

^{a} Values for anisotropically refined atoms are given in the form of the isotropic equivalent displacement parameter defined as $(4/3)[a^2B(1,1) + b^2B(2,2) + c^2B(3,3) + ab(\cos\gamma)B(1,2) + ac(\cos\beta)B(1,3) + bc(\cos\alpha)B(2,3)]$.

(8) Calculations were done on a Local Area MicroVaxII (VAX/VMS V4.6) with the programs SHELX-86 and SHELX-76 and the commercial package SDP.

(9) North, A. C. T.; Philips, D. C.; Matthews, F. S. *Acta Crystallogr., Sect. A: Cryst. Phys., Diffr., Theor. Gen. Crystallogr.* **1968**, *A24*, 351.

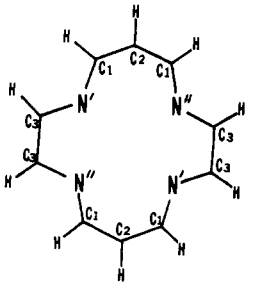

1

the X and Y axes lying in the vertical mirror planes.

The initial molecular potentials for the SCF procedure were obtained by superposition of the Herman–Skillman atomic potentials.[10] The atomic spheres were allowed to overlap, and their radii were taken to be 88.5% of the atomic number radii.[11] The radius of the outer sphere was chosen to touch the outermost atomic sphere radii. The α parameters used were those of Schwarz,[12] and a valence-electron-weighted average was used for the intersphere and outer-sphere regions. The partial wave basis consisted of s-, p- and d-type spherical harmonics on the metal atoms, s and p on N and C, s only on H atoms, and up to $l = 5$ on the outer spheres.

The suitability of the model ligand used in the present calculations has been tested in our previous study of Cr(tmtaa)Cl.[7] The results indicated that the frontier molecular orbitals for a monomer, Cr(tmtaa), calculated with the model ligand as shown in **1**, were very well correlated with those calculated by using the actual ligand and that the character of each MO for the model molecule is very similar to that of the corresponding MO for the actual molecule. Importantly, the same MOs in each case are responsible for metal–metal interaction when the dimer is formed. In the presentation and discussion of the results, we will employ the formula $M_2(tmtaa)_2$ even though the results were actually calculated for the model molecules.

Results

Methods of Preparation. The chromium compound appears to be thermodynamically very favorable. We employed two straightforward methods of preparation, both of which proceed smoothly and in good yield. In addition, three other preparative routes have been mentioned.[3] The preparation of the molybdenum compound was carried out by the general procedure mentioned by Mandon et al.,[2] for which we now give a detailed description. Mandon (private communication) had difficulty in obtaining suitable single crystals and did not, therefore, determine the structure.

Structural Results. We have determined the structure of $Cr_2(tmtaa)_2$ twice, once using the same crystal form as that already mentioned in a preliminary communication[3] but also using a different crystal form. The latter is isomorphous with the crystalline $Mo_2(tmtaa)_2$ that was used for the structure determination. The molecules of $Cr_2(tmtaa)_2$ are essentially identical in the two types of crystal.

Table IV gives lists of the principal molecular dimensions for $Cr_2(tmtaa)_2$ and $Mo_2(tmtaa)_2$ as obtained in the isomorphous crystals. The atoms are labeled in matching fashion so that direct comparisons of the two molecules are easily made. Two views of the $Mo_2(tmtaa)_2$ molecule are shown in Figures 2 and 3. In Figure 2 the labeling of the M and N atoms is defined for use in Table IV. A diagram giving the numbers of all atoms will be found in the supplementary material.

The molecules have no rigorous crystallographic symmetry since they lie on general positions. However, it is evident from Figures 2 and 3 as well as the distances and angles in Table IV that they have effective D_{2d} symmetry, with the mirror planes bisecting opposite pairs of N–M–N angles on each end of the molecule and with the 2-fold axes perpendicular to the M–M axis lying vertically and horizontally in Figure 2.

MO Calculations. The results of the Xα–SW calculations on both $Cr_2(tmtaa)_2$ and $Mo_2(tmtaa)_2$ are summarized in Table V.

(10) Herman, F.; Skillman, S. *Atomic Structure Calculations*; Prentice-Hill: Englewood Cliffs, NJ, 1963.
(11) Norman, J. G., Jr. *J. Chem. Phys.* **1974**, *61*, 4630.
(12) Schwarz, K. *Phys. Rev. B* **1972**, *5*, 2466.

Table III. Positional Parameters and Equivalent Isotropic Thermal Parameters and Their Estimated Standard Deviations for $Mo_2(tmtaa)_2$

atom	x	y	z	B,[a] Å^2
Mo(1)	0.88054 (5)	0.15972 (4)	0.40495 (5)	1.82 (1)
Mo(2)	0.93836 (5)	0.29510 (4)	0.38946 (6)	2.09 (1)
N(1)	0.8546 (5)	0.0997 (4)	0.2359 (5)	2.3 (1)
N(2)	0.6863 (5)	0.1199 (4)	0.3804 (5)	2.1 (1)
N(3)	0.8773 (5)	0.1506 (4)	0.5818 (5)	2.2 (1)
N(4)	1.0466 (5)	0.1295 (4)	0.4394 (5)	2.0 (1)
N(5)	0.7758 (5)	0.3294 (4)	0.3361 (6)	2.9 (2)
N(6)	0.9940 (5)	0.3565 (4)	0.5644 (5)	2.7 (2)
N(7)	1.1337 (5)	0.3318 (4)	0.4366 (6)	2.6 (1)
N(8)	0.9124 (5)	0.2996 (4)	0.2054 (5)	2.5 (1)
C(1)	0.7435 (6)	0.0505 (5)	0.1635 (6)	2.3 (2)
C(2)	0.6299 (7)	0.0348 (5)	0.1897 (7)	2.9 (2)
C(3)	0.6004 (6)	0.0636 (5)	0.2908 (7)	2.6 (2)
C(4)	0.6674 (6)	0.1515 (5)	0.4850 (7)	2.5 (2)
C(5)	0.5655 (7)	0.1780 (6)	0.4831 (8)	3.4 (2)
C(6)	0.5641 (7)	0.2216 (6)	0.5868 (8)	4.4 (2)
C(7)	0.6661 (7)	0.2394 (6)	0.6923 (8)	3.8 (2)
C(8)	0.7677 (7)	0.2130 (5)	0.6945 (7)	3.2 (2)
C(9)	0.7703 (6)	0.1697 (5)	0.5915 (6)	2.4 (2)
C(10)	0.9530 (7)	0.1199 (5)	0.6635 (6)	2.4 (2)
C(11)	1.0551 (7)	0.1019 (5)	0.6440 (6)	2.7 (2)
C(12)	1.1006 (7)	0.1047 (5)	0.5428 (7)	2.4 (2)
C(13)	1.0785 (6)	0.1278 (5)	0.3305 (6)	2.2 (2)
C(14)	1.2018 (7)	0.1496 (5)	0.3255 (7)	3.1 (2)
C(15)	1.2259 (7)	0.1557 (6)	0.2133 (7)	3.6 (2)
C(16)	1.1266 (8)	0.1404 (6)	0.1073 (7)	3.7 (2)
C(17)	1.0022 (7)	0.1198 (5)	0.1115 (7)	3.1 (2)
C(18)	0.9767 (6)	0.1120 (5)	0.2212 (6)	2.3 (2)
C(19)	0.7308 (9)	−0.0015 (6)	0.0486 (8)	4.7 (2)
C(20)	0.4647 (8)	0.0188 (6)	0.2936 (9)	4.5 (3)
C(21)	0.9281 (8)	0.0963 (6)	0.7833 (7)	4.1 (2)
C(22)	1.2119 (7)	0.0722 (5)	0.5604 (7)	3.1 (2)
C(23)	0.7548 (6)	0.3859 (5)	0.4015 (7)	3.0 (2)
C(24)	0.8287 (7)	0.4195 (5)	0.5203 (8)	3.5 (2)
C(25)	0.9386 (7)	0.4080 (5)	0.5961 (7)	3.1 (2)
C(26)	1.1094 (7)	0.3469 (5)	0.6318 (7)	3.0 (2)
C(27)	1.1425 (8)	0.3382 (6)	0.7550 (7)	4.0 (2)
C(28)	1.2532 (9)	0.3183 (6)	0.8113 (9)	5.0 (3)
C(29)	1.3299 (9)	0.3059 (6)	0.7427 (9)	5.1 (3)
C(30)	1.2924 (7)	0.3137 (6)	0.6191 (8)	3.8 (2)
C(31)	1.1861 (7)	0.3340 (5)	0.5630 (7)	2.8 (2)
C(32)	1.1987 (7)	0.3583 (5)	0.3566 (8)	3.3 (2)
C(33)	1.1360 (7)	0.3532 (6)	0.2311 (7)	3.4 (2)
C(34)	1.0100 (7)	0.3288 (5)	0.1619 (7)	3.1 (2)
C(35)	0.7813 (7)	0.2793 (5)	0.1419 (7)	2.7 (2)
C(36)	0.7211 (8)	0.2340 (6)	0.0257 (8)	3.8 (2)
C(37)	0.5882 (9)	0.2077 (6)	−0.0214 (8)	4.5 (3)
C(38)	0.5162 (8)	0.2266 (6)	0.0475 (9)	4.3 (2)
C(39)	0.5752 (7)	0.2677 (5)	0.1630 (8)	3.6 (2)
C(40)	0.7061 (7)	0.2958 (5)	0.2111 (7)	2.9 (2)
C(41)	0.6522 (8)	0.4244 (6)	0.348 (1)	5.2 (3)
C(42)	0.9989 (9)	0.4659 (6)	0.7184 (8)	4.6 (2)
C(43)	1.3416 (8)	0.3968 (7)	0.396 (1)	5.3 (3)
C(44)	0.9845 (9)	0.3419 (7)	0.0270 (8)	5.1 (3)

[a] Values for anisotropically refined atoms are given in the form of the isotropic equivalent displacement parameter defined as $(4/3)[a^2B(1,1) + b^2B(2,2) + c^2B(3,3) + ab(\cos\gamma)B(1,2) + ac(\cos\beta)B(1,3) + bc(\cos\alpha)B(2,3)]$.

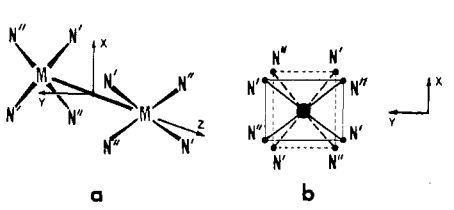

Figure 1. (a) Coordinate system for the MO calculations. The X and Y axes lie in the two vertical mirror planes. Two N_4 planes are both parallel to the XY plane; (b) A view down the Z axis with one N_4 plane above the XY plane and the other below it.

Listed in the table are the MO energies, the relative atomic sphere charge contributions, and the metal atom angular contributions

Table IV. Selected Bond Distances (Å) and Bond Angles (deg) for $Cr_2(tmtaa)_2$ and $Mo_2(tmtaa)_2$

distances	Cr	Mo
M(1)-M(2)	2.101 (1)	2.175 (1)
M(1)-N(1)	2.011 (3)	2.096 (6)
M(1)-N(2)	2.006 (3)	2.095 (6)
M(1)-N(3)	1.997 (3)	2.084 (6)
M(1)-N(4)	2.008 (4)	2.096 (6)
M(2)-N(5)	2.009 (4)	2.091 (7)
M(2)-N(6)	2.009 (3)	2.096 (6)
M(2)-N(7)	2.003 (3)	2.077 (6)
M(2)-N(8)	2.001 (3)	2.088 (6)
M(1) to N(1)-N(4) plane	0.509 (1)	0.560 (1)
M(2) to N(5)-N(8) plane	0.502 (1)	0.549 (1)
angles	**Cr**	**Mo**
M(2)-M(1)-N(1)	105.6 (1)	105.9 (2)
M(2)-M(1)-N(2)	104.9 (1)	106.4 (2)
M(2)-M(1)-N(3)	103.9 (1)	104.9 (2)
M(2)-M(1)-N(4)	104.78 (9)	104.8 (2)
M(1)-M(2)-N(5)	106.9 (1)	107.9 (2)
M(1)-M(2)-N(6)	105.9 (1)	106.2 (2)
M(1)-M(2)-N(7)	103.3 (1)	103.8 (2)
M(1)-M(2)-N(8)	101.9 (1)	103.2 (2)
N(1)-M(1)-N(2)	92.3 (1)	92.7 (2)
N(1)-M(1)-N(3)	150.9 (1)	149.2 (2)
N(1)-M(1)-N(4)	80.4 (1)	79.2 (2)
N(2)-M(1)-N(3)	80.1 (1)	78.7 (2)
N(2)-M(1)-N(4)	150.3 (1)	148.7 (2)
N(3)-M(1)-N(4)	92.5 (1)	92.9 (2)
N(5)-M(2)-N(6)	91.9 (2)	92.6 (3)
N(5)-M(2)-N(7)	149.8 (1)	148.4 (2)
N(5)-M(2)-N(8)	79.9 (2)	78.8 (3)
N(6)-M(2)-N(7)	79.9 (2)	78.1 (3)
N(6)-M(2)-N(8)	152.2 (1)	150.6 (2)
N(7)-M(2)-N(8)	93.8 (1)	94.5 (3)

for the upper valence molecular orbitals. The lower valence MOs that are not listed can be clearly classified, in both cases, as representing the N–C, C–C, and C–H σ bonding. For both molecules, the HOMO and LUMO are the $12b_2$ and $13a_1$ orbitals, respectively. As can be seen clearly from Table V, the calculated molecular orbital diagrams for the two molecules appear to be very similar due to great similarity in their structural features. However, detailed analysis of the results reveals significant differences between the electronic structures of $Cr_2(tmtaa)_2$ and $Mo_2(tmtaa)_2$ as we shall see shortly.

Discussion

This pair of compounds is of particular interest because they afford the opportunity to compare multiple Cr–Cr and Mo–Mo bonds in isostructural compounds in which (a) there are no bridging ligands to constrain the M–M distances and (b) there are no axial ligands to influence the M–M bonding. On the other hand, it must be recognized that the tmtaa ligands do introduce at least two other factors that must be given due consideration in attempting to reach conclusions about the M–M bonding. First, they are bulky enough to cause significant repulsive forces between the halves of the molecule. Second, these ligands have considerable potential for interaction with metal d orbitals through their delocalized π (bonding) and π^* (antibonding) orbitals. We shall pay necessary attention to these factors in the following discussion.

It is worthwhile noting first of all that the steric demands of the two saddle-shaped tmtaa ligands could be (and, we shall later argue, probably *are*) principally responsible for the rotational conformation of the molecules, at least in the case of $Cr_2(tmtaa)_2$. The staggering of the four equivalent benzo groups (and, equally, the four dimethyl-substituted rings) appears to be sterically required, but once done, it provides a very snug internal structure. However, this mandatory arrangement of the ligands automatically leads to the near eclipsing of the two sets of M–N bonds. Therefore, it would be unjustified to infer anything about the strength (or even the existence) of M–M δ bonding from the fact that the M_2N_8 skeleton is eclipsed. Such an inference is justified only in cases (such as $M_2X_8^{n-}$) where rotation to a staggered conformation is not opposed by other forces. This is clearly not the case here.

The Theoretical Analysis. This is one of those instances where it appears most logical (or at least most efficient) to examine the theoretical results first and then consider the experimental facts in detail with the theoretical background in mind.

To begin our examination of the theoretical results, let us take a look at the π orbitals of the NCCCN fragment in the tmtaa ligand because this will facilitate an understanding of the bonding in the molecules. There are three low-lying π orbitals in NCCCN that are already occupied, since the tmtaa ligand is dinegatively charged. Among the π orbitals, the lower two (π_1 and π_2) are π bonding within the fragment and may not be expected to interact significantly with the metal orbitals. The highest (π_3) of the three π orbitals is nonbonding and is formed mainly by the p_π orbitals located on the center C atom and the two N atoms. The four π_3-type orbitals on the two tmtaa ligands can be combined according to a_1, b_2, and e symmetries of the molecular point group. As will be seen below, the π_3-type orbitals of the NCCCN fragments interact strongly with the metal atoms, which results in the M–M bonding scheme in $M_2(tmtaa)_2$ being significantly different from those in the usual quadruply bonded dichromium and dimolybdenum systems.[1]

As shown in Table V, the occupied molecular orbitals for both $Cr_2(tmtaa)_2$ and $Mo_2(tmtaa)_2$ may be divided into two groups according to their main characters. The MO levels below the $10a_1$ orbital represent essentially M–N σ bonding as well as the low-lying π_1 and π_2-type orbitals of the NCCCN fragments. The higher occupied MOs, those from $10a_1$ to $12b_2$ (the HOMO) are responsible for Cr–Cr bonding, Cr–N π bonding, and the π bonding between the C_3 atoms (see **1** for definition of this type of C atom). In the following, our attention will be mainly focused on the molecular orbitals in this second group which determine the M–M bonding and the way in which the M–M bonding is perturbed by metal–ligand π interactions.

$Cr_2(tmtaa)_2$. It is noted from the left part of Table V that the $10a_1$ orbital is contributed by the Cr atoms alone and is predominantly a Cr–Cr σ-bonding orbital. A contour plot of this orbital clearly shows a strong σ-bonding overlap between the pair of d_{z^2} orbitals just as in the well-known cases of quadruply bonded dichromium compounds, e.g., $Cr_2(O_2CH)_4$.[13] The antibonding counterpart of the σ orbital is the unoccupied $13b_2$ orbital. The orbital again has σ^* character similar to that in $Cr_2(O_2CH)_4$ but is also partly Cr–N π antibonding. The Cr–Cr π bonding is distributed over two orbitals of e symmetry, namely, the 17e and 19e orbitals as can be seen from Table V. This partitioning is caused by interaction of the M–M π orbital with the combination of π_3-type orbitals having e symmetry. The features of the Cr–Cr π bonding in both 17e and 19e orbitals as well as the π antibonding presented in the empty 20e orbital are also very similar in appearance to the corresponding cases in $Cr_2(O_2CH)_4$.

The Cr–Cr δ bonding, if it is to occur, should entail the pair of $d_{x^2-y^2}$ orbitals combined with b_2 symmetry. The MOs featuring the δ-type interaction are the $11b_2$ and $12b_2$ orbitals in Table V. The $11b_2$ orbital has 71% metal character, which is mainly from the $d_{x^2-y^2}$ orbitals. Therefore, it should be mainly responsible for the δ bonding. However, as illustrated clearly by the contour plot of this orbital (Figure 4a) plotted in the *XZ* plane, the overlap between the pair of $d_{x^2-y^2}$ orbitals is almost negligible, as compared with that in the corresponding orbital for the $Mo_2(tmtaa)_2$ molecule (Figure 4b). Thus a δ bond of meaningful strength between the pair of Cr atoms is hardly expected, and the eclipsed configuration of the N_4CrCrN_4 framework should be entirely attributed to steric factors.

The nonbonding δ interaction in $Cr_2(tmtaa)_2$ may be considered as a consequence of the bonding interaction between the metal orbitals and the combination of the π_3-type orbitals having b_2 symmetry in the NCCCN fragments. The features of the Cr–N bonding may be seen from the contour plots of the $11b_2$ orbital in different contour planes. Our calculation also shows that the

(13) Cotton, F. A.; Stanley, G. G. *Inorg. Chem.* **1977**, *16*, 2668.

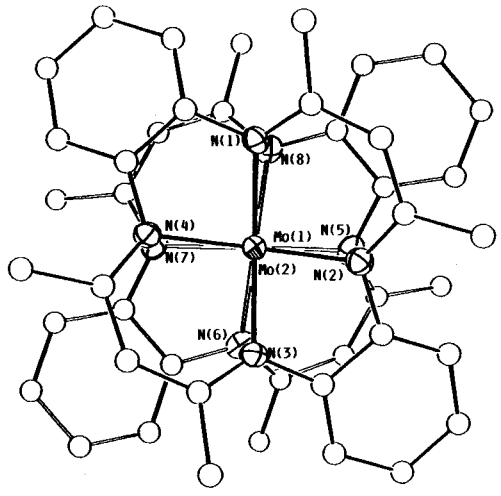

Figure 2. ORTEP view of the $Mo_2(tmtaa)_2$ molecule showing the numbering scheme for the atoms mentioned in Table IV. A fully numbered diagram will be found in the supplementary material. The view here is directly down the M–M axis.

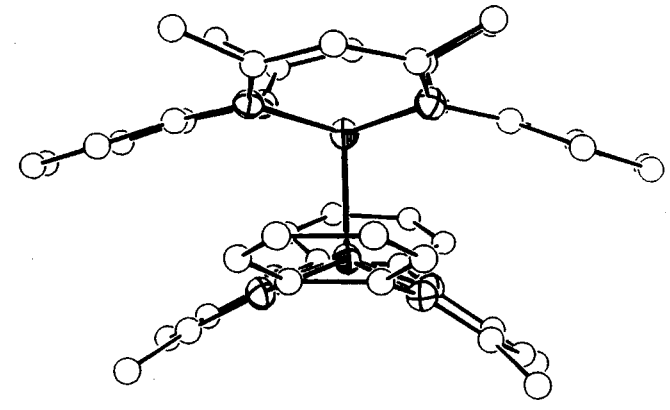

Figure 3. ORTEP diagram of the $Mo_2(tmtaa)_2$ molecule showing how the saddle-shaped ligands fit together snugly.

Table V. Upper Valence Molecular Orbitals for $M_2(tmtaa)_2$ with M = Cr and Mo[a]

$Cr_2(tmtaa)_2$													$Mo_2(tmtaa)_2$										
D_{2d} level	E, eV	% charge								Cr angular contribn			D_{2d} level	E, eV	% charge							Mo angular contribn		
		Cr	N	C_1	C_2	C_3	H_1	H_2	H_3						Mo	N	C_1	C_2	C_3	H_1	H_2	H_3			
$8b_1$	−3.17	9	11	57	0	23	0	0	0				$13b_2$	−3.03	74	18	7	0	1	0	0	0		12% p	87% d
$8a_2$	−3.25	9	12	45	0	33	0	0	0				20e	−3.17	45	21	31	0	3	0	0	0			100% d
$13b_2$	−3.51	81	14	1	3	1	0	0	0		5% p	95% d	$8b_1$	−3.48	2	11	63	0	24	0	0	0			
20e	−3.70	83	8	7	1	1	0	0	0			100% d	$8a_2$	−3.51	2	13	52	0	34	0	0	0			
$13a_1$	−4.80	65	16	0	6	13	0	0	0		2% p	98% d	$13a_1$	−4.67	58	20	0	7	15	0	0	0	1% s	1% p	98% d
$12b_2$	−5.02	52	18	1	13	16	0	0	0		3% p	97% d	$12b_2$	−5.05	39	24	1	16	21	0	0	0		2% p	98% d
$12a_1$	−5.76	53	17	1	8	21	0	0	0	2% s	2% p	96% d	$12a_1$	−5.96	53	19	2	11	15	0	0	0	1% s	1% p	98% d
19e	−5.92	42	27	4	18	9	0	0	0		5% p	95% d	19e	−6.14	31	32	4	19	13	0	0	0		8% p	92% d
$11b_2$	−6.13	71	10	4	10	5	0	0	0			100% d	$11b_2$	−6.56	67	10	5	13	4	0	0	0			100% d
18e	−6.45	4	18	22	0	56	0	0	0				18e	−6.79	1	21	19	4	55	0	0	0			
17e	−6.97	56	12	10	18	4	0	0	0		4% p	96% d	17e	−7.37	45	17	16	17	4	0	0	0		8% p	92% d
$11a_1$	−7.48	3	4	24	30	39	0	0	0				$11a_1$	−7.70	3	6	24	27	40	0	0	0			
$10b_2$	−7.88	2	5	16	19	58	0	0	0				$10b_2$	−8.15	8	5	14	15	58	0	0	0			
$10a_1$	−8.38	98	0	0	0	2	0	0	0	11% s	6% p	83% d	$10a_1$	−9.22	87	6	1	0	5	1	0	0	16% s	4% p	80% d
$7a_2$	−9.33	4	68	23	0	3	1	0	1				16c	−9.61	14	51	11	3	10	8	0	3		29% p	71% d
$7b_1$	−9.58	9	61	18	1	6	2	0	3				$7a_2$	−9.74	3	68	22	0	4	1	0	1			
16e	−9.79	14	46	14	4	9	10	0	3		35% p	65% d	$7b_1$	−9.94	8	62	18	1	6	2	0	3			
15e	−9.89	15	54	9	3	7	7	0	4		33% p	67% d	15e	−10.07	25	46	8	3	9	6	0	3		9% p	91% d
$6a_2$	−10.21	19	36	15	6	9	12	0	3			100% d	$9b_2$	−10.41	8	49	18	5	11	5	0	4			
14e	−10.26	1	53	23	5	16	1	0	0				$9a_1$	−10.49	14	42	16	5	13	4	0	6	14% s	13% p	73% d
$9b_2$	−10.55	4	44	23	7	15	1	0	4				$6a_2$	−10.60	18	36	14	6	10	11	0	4			100% d
$6b_1$	−10.57	15	38	18	7	8	12	0	2			100% d	14e	−10.61	1	56	24	5	12	1	0	0			
$9a_1$	−10.66	8	42	18	5	18	2	0	7				$6b_1$	−10.95	16	35	17	8	10	11	0	2			100% d
13e	−10.94	5	48	19	5	19	3	0	1				13e	−11.30	12	47	16	4	18	0	0	2		3% p	97% d
$8b_2$	−11.31	13	48	12	3	14	9	0	1	56% s		42% d	$8b_2$	−11.35	7	51	14	6	16	5	1	0			
$8a_1$	−11.78	4	19	11	33	11	1	21	0				$8a_1$	−11.82	3	13	12	38	8	0	26	0			

[a] The HOMO is the $12b_2$ orbital in both cases; % charge indicates relative amount of charge in the atomic spheres, and metal angular contribution is given only when >10%.

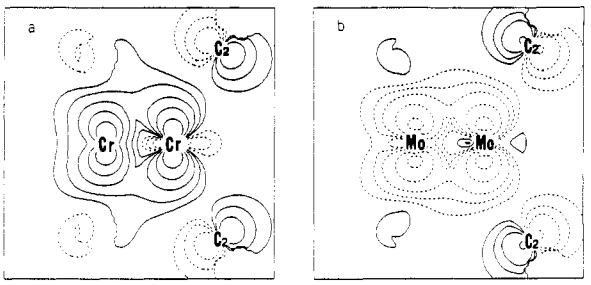

Figure 4. Contour plots of the $11b_2$ orbitals for (a) $Cr_2(tmtaa)_2$ and (b) $Mo_2(tmtaa)_2$. Dashed lines indicate negative contour values. Contour values used in all the plots are as follows: ±0.01, ±0.02, ±0.04, ±0.08, and ±0.16. See text for details of all the plots.

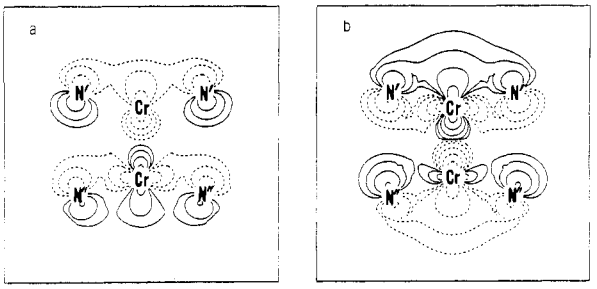

Figure 5. Contour plots of (a) the $11b_2$ orbital and (b) the $12b_2$ orbital for $Cr_2(tmtaa)_2$.

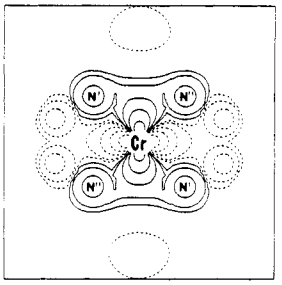

Figure 6. Contour plot of the $12a_1$ orbital for $Cr_2(tmtaa)_2$.

orbitals of δ-type have been mixed more or less with the M–M σ^* character (also b_2 symmetry). Thus Figure 5a illustrates the Cr–N bonding due to overlap of the σ^* component mixed in the orbital with the p_π orbitals on the N atoms. The orbital was plotted on a plane containing the Cr–Cr axis (*Z* axis) and two N′ atoms bonded to one Cr atom (see also Figure 1). The two N″ atoms bonded to another Cr atom are actually not on the contour plane but are very close to it (Figure 1). The p_π orbitals on the N atoms can also have certain overlap with the $d_{x^2-y^2}$ component in the $11b_2$ orbital. This is well shown by the contour plot in Figure 6 which is plotted for the $12a_1$ orbital discussed below. The contour plane in this figure was chosen to be parallel to the *XY* plane and contain a Cr atom at the center. The N atoms labeled in Figure 6 are not in the contour plane but in a N_4 plane just 0.51 Å above the contour plane. They are labeled only for the purpose of indicating clearly the overlap between the $d_{x^2-y^2}$ orbital and the N p_π orbitals, which are approximately vertically located on the N_4 plane. The $12b_2$ orbital, which is the HOMO in $Cr_2(tmtaa)_2$, on the other hand, has been significantly mixed with the Cr–Cr σ^* character. Thus the orbital is primarily involved in the Cr–N π bonding, as shown by its contour plot in Figure 5b plotted in the same plane as that in Figure 5a. It may be noticed that the Cr–N bonding just discussed, although unfavorable for the Cr–Cr δ bonding, obviously enhances the bonding of the metal atoms to the ligands.

The δ^*-type interaction is distributed in the $12a_1$ and $13a_1$ orbitals in Table V, both of which have a metal contribution from $d_{x^2-y^2}$ orbitals. The $12a_1$ orbital, which is lower in energy than the HOMO, is again involved in the Cr–N bonding due to the interaction of the metal orbitals with the π_3-type orbitals of the NCCCN fragments combined with a_1 symmetry. The bonding is shown by the contour plot of the orbital in Figure 6 and is very similar to that in the $11b_2$ orbital. The $13a_1$ orbital, on the other hand, can be regarded as the Cr–N antibonding counterpart of the $12a_1$ orbital. This is the LUMO for $Cr_2(tmtaa)_2$, and it is only 0.2 eV higher than the HOMO. Finally, it may be worth mentioning that the significant involvement of the HOMO and LUMO in the metal–ligand interaction predicted by the calculation helps us to understand the observed weak paramagnetism (0.49 μB/Cr)[3] of $Cr_2(tmtaa)_2$. If the magnetism resulted only from the absence of a δ bond due to a nonbonding δ-type HOMO with little ligand character, stronger magnetism than that actually observed would be expected, since the LUMO would be also nonbonding but of δ^* type, without ligand character and very close in energy to the HOMO.

Table VI. Comparison of Representative Cr–Cr and Mo–Mo Distances[a]

compd type	M–M dist, Å		
	Mo–Mo	Cr–Cr	Δ
$[M_2(CH_3)_8]^{4-}$	2.148 (2)	1.980 (5)	0.168
$M_2(O_2CCH_3)_4$	2.079 (3)[b]	1.97 (1)[b]	0.11
$M_2(C_3H_5)_4$	2.183 (2)	~1.97	0.21
$M_2[(CH_2)_2PMe_2]_4$	2.082 (2)	1.895 (3)	0.187
$M_2[2,6\text{-}(CH_3O)_2C_6H_3]_4$	2.064 (1)	1.847 (1)	0.217
$M_2(mhp)_4$	2.065 (1)	1.889 (1)	0.176
$M_2[(xylyl)NCMeO]_4$	2.083 (2)	1.937 (2)	0.146

[a] For abbreviations and sources of data see ref 1. [b] These values are for the gas phase, measured by electron diffraction: Ketkar, S. N.; Fink, M. *J. Am. Chem. Soc.* **1985**, *107*, 338 and references therein.

$Mo_2(tmtaa)_2$. As mentioned before, the MOs of this molecule are very similar to those of $Cr_2(tmtaa)_2$. In fact, the Mo–Mo σ- and π-bonding orbitals as well as the Mo–N bonding orbitals have almost the same characters and shapes as those in the Cr compound. However, a significant difference appears in the electronic structures of the two molecules due to the existence of appreciable δ bonding between the molybdenum atoms. As can be seen in Figure 4b, there is sufficient overlap between the $4d_{x^2-y^2}$ orbitals to indicate unambiguously that a Mo–Mo δ bond exists. This is in sharp contrast to the much weaker overlap between the $3d_{x^2-y^2}$ orbitals in Figure 4a for $Cr_2(tmtaa)_2$. The difference can be attributed to the fact that the 4d orbitals, which are more diffuse than the 3d orbitals, have poorer overlap with the ligand π orbitals but better overlap with each other. Consequently, the dimolybdenum complex is still a quadruply bonded system, while there is approximately only a triple bond in $Cr_2(tmtaa)_2$.

It is also important to note that the calculated HOMO–LUMO energy gap is doubled in the Mo molecule compared with that calculated for the Cr molecule. Thus, we can explain why the Cr molecule shows weak paramagnetism at room temperature while at the same time suggest that the Mo compound is likely to be fully diamagnetic. Clearly, a detailed study of the magnetism as a function of temperature would be of interest, especially for $Cr_2(tmtaa)_2$.

We turn now to the interpretation of the M–M bond lengths. First, the Cr–Cr bond length of 2.101 (1) Å is long compared to those found in a number of Cr_2^{4+} compounds, as shown by the typical values in Table VI. There are two reasons for this. For one thing, the ligands on the two metal atoms, although well fitted to each other, presumably make repulsive contacts that resist any closer approach. Second, as the MO calculations have shown, there is essentially no δ bonding between the Cr atoms; thus, this is only a triple Cr–Cr bond.

Another point of comparison is that the Mo–Mo bond length exceeds the Cr–Cr bond length by only 0.074 Å. This is less than the differences found in other pairs of homologous Cr_2^{4+}/Mo_2^{4+} compounds, as shown in Table VI. The Mo–Mo bond itself is actually a little longer than the values found in many other unbridged Mo_2^{4+} compounds, so that the smallness of the difference is due entirely to the fact that the Cr–Cr distance is increased by the two factors discussed in the previous paragraph.

Finally, we can compare the $Mo_2(tmtaa)_2$ molecule with the $[Mo_2(tmtaa)_2]^+$ ion, whose structure is already known.[2] There is no important difference between the two, other than the increase

in the Mo–Mo distance, 0.046 Å. This increase is entirely consistent with those previously seen in similar circumstances, namely, where one δ electron is removed from an Mo–Mo $\sigma^2\pi^4\delta^2$ configuration. In the first such case, $[Mo_2(SO_4)_4]^{4-}$ to $[Mo_2(SO_4)_4]^{3-}$, the increase was 0.056 Å,[14] and more recently for $Mo_2(tolNCHNtol)_4$ to $[Mo_2(tolNCHNtol)_4]^+$, the increase was 0.037 Å.[15]

Acknowledgment. We thank the National Science Foundation for support.

Supplementary Material Available: Fully labeled ORTEP drawings of compounds I and II, listings of the positional parameters for the hydrogen atoms in compound I, and full tables of anisotropic displacement parameters and bond angles and distances for compounds I and II (21 pages); listings of observed and calculated structure factors for I and II (44 pages). Ordering information is given on any current masthead page.

(14) Cotton, F. A.; Frenz, B. A.; Pedersen, E.; Webb, T. R. *Inorg. Chem.* **1975**, *14*, 391.

(15) Cotton, F. A.; Feng, X.; Matusz, M. *Inorg. Chem.* **1989**, *28*, 594.

Contribution from the Departments of Chemistry, SUNY Cortland, Cortland, New York, 13045, University of Virginia, Charlottesville, Virginia 22901, and James Madison University, Harrisonburg, Virginia 22807

Luminescence Studies of Pyridine α-Diimine Rhenium(I) Tricarbonyl Complexes†

LouAnn Sacksteder,‡ Arden P. Zipp,*,§ Elizabeth A. Brown,‡ Julie Streich,§ J. N. Demas,*,‡ and B. A. DeGraff*,⊥

Received January 2, 1990

The room- and low-temperature luminescences of $ReL(CO)_3X$ where L = 2,2'-bipyridine, 1,10-phenanthroline, or 5-phenyl-1,10-phenanthroline and X = substituted pyridine or quinoline were studied. Relatively small but useful variations in the state energies can be effected by altering the Hammett σ values of substituents on the pyridines. All complexes exhibit metal to ligand charge-transfer (MLCT) phosphorescences at room temperature. However, by choice of suitable ligands, the emissions can be switched to ligand-localized phosphorescence on cooling to 77 K. This behavior is explained on the basis of the proximity of the lowest MLCT and π–π^* triplet states and the changes in energy of the MLCT state as a function of temperature. At room temperature the MLCT state can equilibrate to an energy that is lower than that of $^3\pi$–π^* state and give MLCT luminescence. In rigid low-temperature media, however, the MLCT state cannot relax during the excited-state decay and emission is from the lower energy $^3\pi$–π^* state. At room temperature, lifetimes are predominantly affected by alterations in the nonradiative rate constant, as described by the energy-gap law. From σ values of the substituents, both state energies and lifetimes can be predicted before synthesis. The design of new luminescent complexes is discussed.

Introduction

Luminescent d^6 transition-metal complexes are useful as probes of macromolecular structures[1] and heterogeneous media,[2] as well as photosensitizers for solar energy conversion[3] and electron-transfer reactions.[4] While Ru(II) complexes, in particular, have been used most widely in these applications, the excited-state properties of complexes of Re(I),[5,6] Ir(III),[7] Mo(0), W(0),[8] and Os(II),[9] have been increasingly investigated. Since the metal, ligands, and solvent environment can all affect excited-state properties, variations of one or more of these factors can be used to "tune" the photophysical and photochemical properties.[10-12]

A particularly important class of luminescent complexes has been *fac*-$ReL(CO)_3X$ where L is an α-diimine ligand and X can be varied from simple ions such as Cl, Br, and CN to organic ligands such as pyridine. As part of our interest in designing specially tailored luminescent metal complexes as probes, we have examined the luminescence properties of a series of complexes where X is a substituted pyridine. We wished to determine to what extent varying the pyridine would affect the state energies, the energy degradation paths, and the radiative and nonradiative rates in the complexes.

By variation of the substituents, the basicity of the pyridines can be manipulated over 7 orders of magnitude. Given the previously demonstrated sensitivity of $ReL(CO)_3NCR^+$ to subtle structural variations in the R group,[13] we anticipated that altering the pyridines would yield large changes in the luminescence properties. We find that variations in the pyridines have a much smaller effect on the luminescence properties than we had anticipated on the basis of the wide range of electron-donor and -acceptor substituents employed. However, useful variations in properties can be effected by suitably varying the pyridine ligands.

† Presented in part at the 17th Northeast Regional Meeting of the American Chemical Society in Rochester, NY, on Nov 8-11, 1987.

‡ University of Virginia.
§ SUNY Cortland.
⊥ James Madison University.

(1) (a) Kumar, C. V; Barton, J. K.; Turro, N. J. *J. Am. Chem. Soc.* **1985**, *107*, 5518. (b) Barton, J.; Lolis, E. *J. Am. Chem. Soc.* **1985**, *107*, 708. (c) Barton, J. K.; Danishefsky, A. T.; Goldberg, J. M. *J. Am. Chem. Soc.* **1984**, *106*, 2172. (d) Barton, J. K.; Basik, L. A.; Danishefsky, A. T.; Alexandrescu, A. *Proc. Natl. Acad. Sci. U.S.A.* **1984**, *81*, 1961.

(2) Kalyanasundaram, K. *Photochemistry in Microheterogeneous Systems*; Academic Press: New York, 1987.

(3) (a) *Energy Resources through Photochemistry and Catalysis*; Grätzel, M., Ed.; Academic Press: New York, 1983. (b) Kalyanasundaram, K. *Coord. Chem. Rev.* **1982**, *46*, 159. (c) Balzani, V.; Bolletta, F.; Gandolfi, M. T.; Maestri, M. *Top. Curr. Chem.* **1978**, *75*, 1.

(4) (a) Creutz, C.; Sutin, N. *Proc. Natl. Acad. Sci. U.S.A.* **1975**, *72*, 2858. (b) Lin, C.; Sutin, N. *J. Phys. Chem.* **1976**, *80*, 97.

(5) (a) Caspar, J. V.; Sullivan, B. P.; Meyer, T. J. *Inorg. Chem.* **1984**, *23*, 2104. (b) Caspar, J. V.; Meyer, T. J. *J. Phys. Chem.* **1983**, *87*, 952.

(6) (a) Wrighton, M. S.; Morse, D. L. *J. Am. Chem. Soc.* **1974**, *96*, 998. (b) Luong, J. C.; Faltynak, H.; Wrighton, M. S. *J. Am. Chem. Soc.* **1979**, *101*, 1597. (c) Giordano, P. J.; Fredericks, S. M.; Wrighton, M. S.; Morse, D. L. *J. Am. Chem. Soc.* **1978**, *100*, 2257. (d) Fredericks, S. M.; Luong, J. C.; Wrighton, M. S. *J. Am. Chem. Soc.* **1979**, *101*, 7415. (e) Giordano, P. J.; Wrighton, M. S. *J. Am. Chem. Soc.* **1979**, *101*, 2888.

(7) (a) Watts, R. J.; Brown, M. J.; Griffith, B. G.; Harrington, J. S. *J. Am. Chem. Soc.* **1975**, *97*, 6029. (b) Watts, R. J.; Griffith, B. G.; Harrington, J. S. *J. Am. Chem. Soc.* **1976**, *98*, 674.

(8) (a) Lees, A. J. *Chem. Rev.* **1987**, *87*, 711. (b) Connor, J. A.; Overton, C.; El Murr, N. *J. Organomet. Chem.* **1984**, *277*, 277. (c) Connor, J. A.; Overton, C. *Inorg. Chim. Acta* **1982**, *65*, L1. (d) Abrahamson, H. B.; Wrighton, M. S. *Inorg. Chem.* **1978**, *17*, 3385. (e) Wrighton, M. S. *Chem. Rev.* **1972**, *74*, 401.

(9) (a) Kober, E. M.; Marshall, J. L.; Dressick, W. J., Sullivan, B. P.; Caspar, J. V.; Meyer, T. J. *Inorg. Chem.* **1985**, *24*, 2755. (b) Caspar, J. V.; Kober, E. M.; Sullivan, B. P.; Meyer, T. J. *J. Am. Chem. Soc.* **1982**, *104*, 630. (c) Kober, E. M.; Sullivan, B. P.; Dressick, W. J.; Caspar, J. V.; Meyer, T. J. *J. Am. Chem. Soc.* **1980**, *102*, 1383.

(10) (a) Watts, R. J.; Crosby, G. A. *J. Am. Chem. Soc.* **1971**, *93*, 3184. (b) Malouf, G.; Ford, P. C. *J. Am. Chem. Soc.* **1977**, *99*, 7213. (c) Ford, P. C. *Rev. Chem. Intermed.* **1979**, *2*, 267.

(11) (a) Pankuch, B. L.; Lackey, D. E.; Crosby, G. A. *J. Phys. Chem.* **1980**, *84*, 2061. (b) Pankuch, B. J.; Lackey, D. E.; Crosby, G. A. *J. Phys. Chem.* **1980**, *84*, 2068.

0020-1669/90/1329-4335$02.50/0